MEMS-based multi-modal vibration energy harvesters for ultra-low power autonomous remote and distributed sensing

Iannacci, J.; Serra, E.; Sordo, G.; Bonaldi, M.; Borrielli, A.; Schmid, U.; Schneider, M.; Pandraud, G.; Sarro, P. M.; More Authors

DOI
10.1007/s00542-018-3923-1

Publication date
2018

Document Version
Final published version

Published in
Microsystem Technologies

Citation (APA)
Iannacci, J., Serra, E., Sordo, G., Bonaldi, M., Borrielli, A., Schmid, U., Schneider, M., Pandraud, G., Sarro, P. M., & More Authors (2018). MEMS-based multi-modal vibration energy harvesters for ultra-low power autonomous remote and distributed sensing. *Microsystem Technologies*, *24*(12), 5027-5036. https://doi.org/10.1007/s00542-018-3923-1

Microsystem Technologies (2018) 24:5027–5036
https://doi.org/10.1007/s00542-018-3923-1

TECHNICAL PAPER

MEMS-based multi-modal vibration energy harvesters for ultra-low power autonomous remote and distributed sensing

J. Iannacci[1] · E. Serra[2,3] · G. Sordo[1] · M. Bonaldi[2,4] · A. Borrielli[2,4] · U. Schmid[5] · A. Bittner[5] · M. Schneider[5] · T. Kuenzig[6] · G. Schrag[6] · G. Pandraud[3] · P. M. Sarro[3]

Received: 16 April 2018 / Accepted: 23 April 2018 / Published online: 2 May 2018

Abstract
In this contribution, we discuss the implementation of a novel microelectromechanical-systems (MEMS)-based energy harvester (EH) concept within the technology platform available at the ISAS Institute (TU Vienna, Austria). The device, already presented by the authors, exploits the piezoelectric effect to convert environmental vibrations energy into electricity, and presents multiple resonant modes in the frequency range of interest (i.e. below 10 kHz). The experimental characterisation of a sputter deposited aluminium nitride piezoelectric thin-film layer is reported, leading to the extraction of material properties parameters. Such values are then incorporated in the finite element method model of the EH, implemented in Ansys Workbench^{TM}, in order to get reasonable estimates of the converted power levels achievable by the proposed device solution. Multiphysics simulations indicate that extracted power values in the range of several μW can be addressed by the EH-MEMS concept when subjected to mechanical vibrations up to 10 kHz, operating in closed-loop conditions (i.e. piezoelectric generator connected to a 100 kΩ resistive load). This represents an encouraging result, opening up the floor to exploitations of the proposed EH-MEMS device in the field of wireless sensor networks and zero-power sensing nodes.

1 Introduction

Remote and distributed sensing is becoming the turning point of novel applications aimed to improve people quality of life, in particular for ageing society, through enhanced connectivity based services. Nowadays, acronyms like internet of things (IoT) (Coetzee and Eksteen 2011) and ambient assisted living (AAL) (Prescher et al. 2012) are important driving forces in research and applications. Massive exploitation of small, smart and capillary distributed wireless sensor networks (WSNs) (Hackmann et al. 2014), i.e. the building blocks of the afore-mentioned scenarios, poses critical demands in terms of power availability to ensure proper operation. Batteries [traditional or super-capacitor based (Karangia et al. 2013)] are the most diffused solution to power sensing nodes, despite intrinsic limitations in terms of long-time duration and miniaturisation. On the other hand, the field of energy harvesting (EH) (Wan et al. 2011) has proven in the last decade to be a valuable solution to extract energy from environmental sources, like mechanical vibrations, thermal gradients, electromagnetic waves, etc., and to make it available to the systems/devices to be powered. Given the trends of integration, miniaturisation and ultra-low power (ULP) consumption followed by WSNs applications, microelectromechanical-systems (MEMS) technology is being investigated to manufacture energy harvesters (EHs) (Priya and Inman 2009), decreasing the achievable power levels addressed by traditional devices, despite pushing

✉ J. Iannacci
iannacci@fbk.eu

1 Center for Materials and Microsystems (CMM), Fondazione Bruno Kessler (FBK), Povo, Trento, Italy

2 Gruppo Collegato di Trento, Istituto Nazionale di Fisica Nucleare (INFN), Povo, Trento, Italy

3 DIMES Technology Center, Delft University of Technology, Delft, The Netherlands

4 Nanoscience-Trento-FBK Division, Institute of Materials for Electronics and Magnetism, Povo, Trento, Italy

5 Institute of Sensor and Actuator Systems (ISAS), Vienna University of Technology (TUW), Vienna, Austria

6 Institute for Physics of Electrotechnology (TEP), Munich University of Technology (TUM), Munich, Germany

significantly down dimensions and opening, in turn, the floor to hybridisation of active sensing electronics and power supply on the same chip (Iannacci 2017).

Vibration based EH, i.e. the conversion of mechanical energy scattered in the environment into electrical energy, represents a research stream of particular interest in modern wireless devices and networks. Starting from the mid-90s, the interest of research commenced to focus on the realisation of energy autonomous strategies for electronic devices. The solution reported in Kymissis et al. (1998) exploits a piezoelectric energy converter housed in athletic shoes, and is one of the first relevant examples of environmental EH devoted to powering electronic modules (Iannacci and Sordo 2015). Since then, research on vibration based EH devices took significant steps forwards, fed by the continuous trend of decreasing power consumption in integrated circuits (ICs), making the scenario of self-powered (wireless) devices (Roundy et al. 2004) and traditional batteries replacement possible. Given these considerations, next challenges for vibration EHs are, namely, miniaturisation and integration with active electronics, opening up the floor to a massive exploitation of MEMS and microsystems technologies.

Common vibration to electrical power conversion methods for EH-MEMS are basically three: piezoelectric, electromagnetic and electrostatic (Kamierski and Beeby 2010). In the first case, the piezoelectric effect is exploited to extract electricity from the mechanical vibration of a suspended proof mass (Erturk and Inman 2011). In electromagnetic scavengers, instead, the oscillation of a permanent magnet induces an electric current into a coil (Tao et al. 2012). Finally, the electrostatic transduction is based on charge displacement in two capacitor electrodes in relative movement to each other (Liu et al. 2012; Iannacci et al. 2013b; Solazzi et al. 2011). Obviously, shrinking down dimensions from macro- to micro-domain brings a dowry of numerous pros and cons. First, scaling down devices footprint means reducing the harvested power, it looking at first sight as a limiting constraint. Nonetheless, if, on one side, supply of low-power and ULP electronics is less and less demanding (as mentioned above), on the other hand, development of micro-fabrication technologies enables to enhance energy conversion efficiency of MEMS-based vibration EHs. To this end, piezoelectric conversion in the micro-domain exhibits power densities that are even larger than traditional macro-devices, as reported in Zhu (2011). Differently, electromagnetic (Cugat et al. 2003) and electrostatic micro-devices are in general less performing, despite also less mature, if compared to piezoelectric solutions (Zhu 2011), and thereby still admit considerable margins of improvement.

Another issue arising from miniaturisation of EHs is the scaling of operating frequency. As is well-known, resonant frequency of a vibrating device increases when its mass and geometry are shrunk (Kamierski and Beeby 2010), while most part of ambient vibration energy is available below a few kHz (e.g. busy street, car engine, industrial/domestic appliance, etc.) (Roundy et al. 2004). State of the art solutions to circumvent this problem are available, them being based on up conversion of ambient vibration frequency until reaching the converter resonance. For instance, this is achieved by exploiting complementary magnets (Galchev et al. 2012), or by designing the mechanical structure so that snap (Fu et al. 2012; Zorlu et al. 2011) and buckling induced pulses (Chamanian et al. 2012) are imposed to the micro-converter. Additional solutions directed to widen vibration EHs spectrum of sensitivity are also discussed in literature. By making the elastic behaviour of a vibrating mass non-linear, the device frequency response exhibits a chaotic behaviour (duffing mode resonance) (Halvorsen 2013), extending the frequency range of operability and, in turn, the level of extracted power (Hajati et al. 2011; Goldschmidtboeing et al. 2009). Moreover, tuning of EHs resonant frequency is also studied to maximise extraction in the widest possible range of operability (Todorov et al. 2011).

Concerning technology, the scientific literature is populated by findings in the field of material science and thin-film deposition techniques, resulting in relevant improvements in power conversion of vibration EHs. Starting from piezoelectric materials, the optimisation of deposition conditions (e.g. temperature, grain growth) (Akiyama et al. 2009; Zukauskaite et al. 2012) and in patterning of layers (i.e. interdigitated) (Chidambaram et al. 2012) reflects in large enhancements of piezoelectric response. Concerning electrostatic (i.e. capacitive) EHs, conversion capabilities are importantly boosted by deposition of densely charged electrets, i.e. permanently charged/polarised dielectric layers (Hagiwara et al. 2012; Suzuki et al. 2011). Finally, miniaturised electromagnetic EHs, previously considered to be not successful because of scaling issues (Cugat et al. 2003), recently started to benefit from the development of efficient techniques for patterning (Miki et al. 2012) and bonding (Tao et al. 2012) of thin layers with improved magnetic properties, increasing the magnet-to-coil coupling, and, in turn, the EHs performance.

Given the rather wide scenario depicted above, the focus of this work is confined around the operability extension of MEMS-based harvesting devices, achieved by means of the pronounced converter sensitivity distributed on a wide range of excitation frequencies. This target can be reached by referring to a couple of different fashions. On one side, redundant employment of MEMS resonators with varied suspended mass and/or elastic constant extends frequency operation of the whole array (Chandrahalim and Bhave 2008). On the other hand, another viable solution consists

in designing the MEMS mechanical structure in such a way to exhibit a large number of resonant modes in a certain frequency range (i.e. multi-modal resonant structure) (Brennen et al. 1990; Casset et al. 2009).

The paper is arranged as follows. Section 2 discusses the work developed by the authors, framing the context of the following activity reported in this paper. Section 3 briefly introduces the technology for the fabrication of the discussed EH-MEMS concept and then focuses on the experimental activities carried out around the characterisation of thin-films with piezoelectric properties. Section 4 discusses the details concerning multiphysics simulations of the proposed EH-MEMS concept, also comprising the piezoelectric conversion effect and estimates of the achievable harvested power levels. Section 5 eventually reports some final considerations and further perspectives for the future development of this work.

2 Developed work

The authors already discussed the development of high-performance, wide-band MEMS-based vibration EH devices (Iannacci et al. 2014). The solution we propose is based on a circular shaped Silicon suspended mass (diameter of 6–8 mm; thickness in the range of 300–500 μm) named four-leaf clover (FLC). It presents multiple resonant modes (i.e. multi-modal resonator) in the below-10 kHz vibration frequency range, which is where most part of the scattered energy is distributed (e.g. busy streets, car engines, industrial/domestic appliances, etc.). The FLC EH-MEMS is conceived to transform vibrations into electric energy through piezoelectric conversion mechanism. Physical samples of the sole FLC mechanical resonator have been manufactured at the DIMES Technology Center (The Netherlands) (see Fig. 1) and tested at Munich University of Technology (Germany) (Iannacci et al. 2014), showing resonances already starting from 300 to 400 Hz in ambient pressure conditions. Finite element method (FEM) simulations performed in Ansys Workbench™ have been confronted against experimental results for validation purposes, proving the good accuracy achievable with the selected analysis methodology in predicting the mechanical dynamic behaviour (i.e. resonant modes).

Optimised samples of FLC designs were realised in the microfabrication facility of the ISAS Institute (TU-Vienna, Austria) also including high-performance aluminium nitride (AlN) piezoelectric layer, leading to the realisation of complete MEMS-based EH converters (Iannacci et al. 2016), as discussed below.

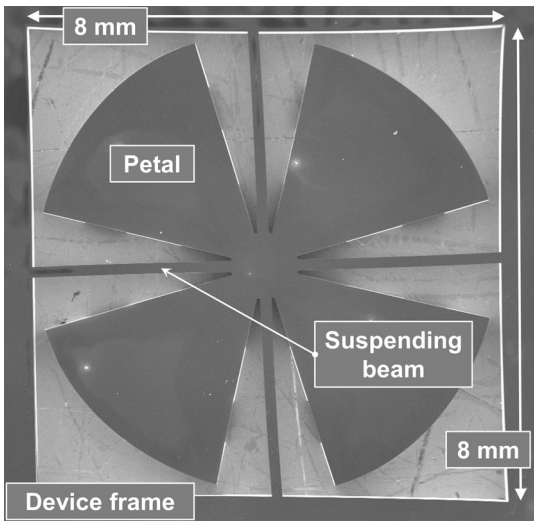

Fig. 1 SEM (scanning electron microscopy) photograph of an FLC physical sample (sole mechanical resonator) fabricated at the DIMES Technology Center (Iannacci et al. 2014)

3 Experimental characterisation of aluminium nitride piezoelectric layer

A suitable technology for the manufacturing of FLC EH-MEMS was described in Iannacci et al. (2014) and is based on double etching (front-/back-side) of silicon on insulator (SOI) wafers with deep reactive ion etching (DRIE), for the release of deformable springs (thin silicon) and proof masses (thick silicon). Concerning the piezoelectric thin-film, it has to be deposited on the front side of the device and must be sandwiched between two metal layers (bottom and top) in order to ensure redistribution of electrical signals. Such technology process is available at ISAS Institute (Vienna), and the focus of this section is spent around the experimental characterisation of mechanical properties of sputter deposited AlN.

In order to determine the mechanical properties such as film stress and Young's modulus of AlN thin-films, a load deflection method is applied. Using this approach, the bending curve of a freestanding, circumferentially-clamped diaphragm under a uniformly distributed differential pressure load p_m is measured. The pressure is applied using a syringe pump system, which is described in more details in Schalko et al. (2011). The bending curve is measured by a white light interferometer from Polytec (http://www.polytec.com). The membrane is fabricated by sputtering a 366 nm thin AlN film on a silicon wafer covered with Silicon oxide layer. During deposition the chamber pressure was $p = 6$ μbar, substrate-target distance $d_{ST} = 65$ mm and plasma power $P = 800$ W, respectively. Using standard processing techniques, the membrane is created by DRIE etch step. The measurement is then analysed using a new analytical model described in

Schalko et al. (2011). The measured bending curve is fitted using the following polynomial expression

$$w(r) = w_0\left[1-\left(\frac{r}{R}\right)^2\right]\left[1+\sum_{m=1}^{M}\alpha_{2m}\left(\frac{r}{R}\right)^{2m}\right] \quad (1)$$

with the membrane radius R, the measured bending curve $w(r)$ and the maximum displacement w_0. The coefficients α_{2m} are the fit parameters, determined by the bending shape. Using $M = 2$ yields a good agreement between (1) and the measurement, as shown in Fig. 2.

Applying different pressures p_m and measuring $w_0(p_m)$, the standard bulge-test equation

$$p_m(w_0) = C_1(\alpha_{2m})\frac{\sigma_f d w_0}{R^2} + C_2(\nu, \alpha_{2m})\frac{Y d w_0^3}{R^4} \quad (2)$$

can be applied to determine the film stress σ_f and the Young's modulus Y. The coefficients C_1 and C_2 are derived from α_{2m} according to Schalko et al. (2011) with the Poisson's ratio fixed at $\nu = 0.24$ (Sah et al.2010). The film thickness is denoted by d and measured to $d = 366$ nm. Figure 3 shows an excellent agreement between measurement and theory as well as a good reproducibility.

The stress is determined to be $\sigma_f = (285 \pm 15)$ MPa and the Young's modulus is $Y = (227 \pm 10)$ GPa. Those values are smaller than those obtained for bulk-AlN (Wagner and Bechstedt 2002), which can be attributed to effects related to specific microstructure and the film thickness.

4 Multiphysics simulations

As mentioned in Sect. 2, a multiphysics simulation procedure based on Ansys Workbench was set up for FLC devices and validated against experimental results (Iannacci et al. 2014). In this section, such a methodology is exploited in order to assess the extracted power levels achievable with the discussed EH-MEMS design concept.

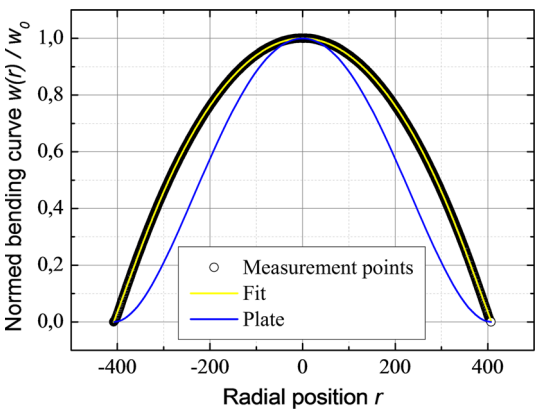

Fig. 2 Normalised bending curve. The lines show the fit of the theoretical model compared to pure plate behaviour

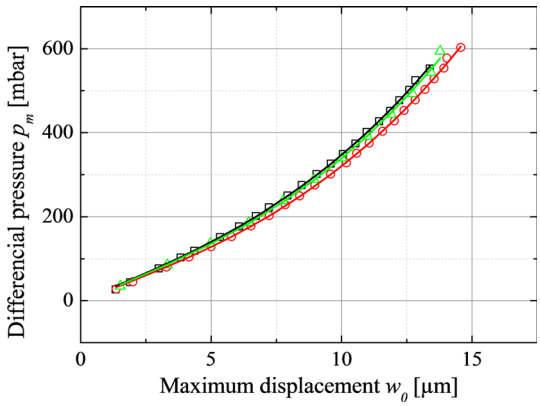

Fig. 3 Load-deflection curves measured for three different samples showing excellent agreement between measurement and theory as well as good reproducibility

As already pointed out before, full processing of physical FLC EHs comprised of AlN piezoelectric layer is performed at the ISAS Institute (Vienna) (Sordo et al. 2015, 2016a, b). Thereafter, all the simulations reported in this section are tailored to the material properties and geometry features typical of such technology platform.

The geometry features of the simulated FLC device are listed in Table 1, while details of the double mass–spring systems (m_1, k_1; m_2, k_2) realised by each petal are visible in the schematic reported in Fig. 4.

The thickness of the FLC flexible spring parts and of the proof masses are compliant with the SOI 4 inch wafer typically employed at ISAS, while thickness and properties of AlN layer are those mentioned in Sect. 3. It must be noted that the detailed FLC configuration does not represent an optimised design but rather a pilot device that will be further improved before being physically manufactured.

While modal (eigenfrequency) analysis allows to extract resonant frequencies (Iannacci et al. 2013a), it does not enable to couple the mechanical and electrical domains. Thereafter, we chose to perform harmonic simulations with the target to observe the FLC power output in response to a mechanical stimulus imposed to the resonant structure. Sketching of the parameterised 3D FLC model, definition of boundary conditions (e.g. mechanical constraints and stimuli) and mechanical properties of materials are manageable within the Ansys Workbench environment (ANSYS Inc. 2012a). Conversely, the piezoelectric effect is defined in Ansys Classic. The Workbench tool offers the possibility to integrate sets of Ansys Parametric Design Language commands (APDL) (ANSYS Inc. 2012b) in the simulation flow, enabling the coupled-field analysis of piezoelectric materials. Figure 5 highlights the project tree in the graphical user interface (GUI) of Ansys Workbench, within which we added three sections of APDL commands in order to model the AlN piezoelectric layer.

Table 1 Geometry features of the FLC EH-MEMS simulated in Ansys Workbench

Geometry feature	Value
Suspending beam length (X-axis)	4100 μm
Suspending beam width (Y-axis)	120 μm
Suspending beam thickness (Z-axis)	20 μm
Radius of petals	4000 μm
Angular aperture of petals	30°
Length of inner flexible petals membrane (k_1) along radius	1500 μm
Length of outer flexible petals membrane (k_2) along radius	750 μm
Length of inner petals proof mass (m_1) along radius	1000 μm
Length of outer petals proof mass (m_2) along radius	750 μm
Thickness of flexible petals membranes (k_1 and k_2)	20 μm
Thickness of petals proof masses (m_1 and m_2)	350 μm

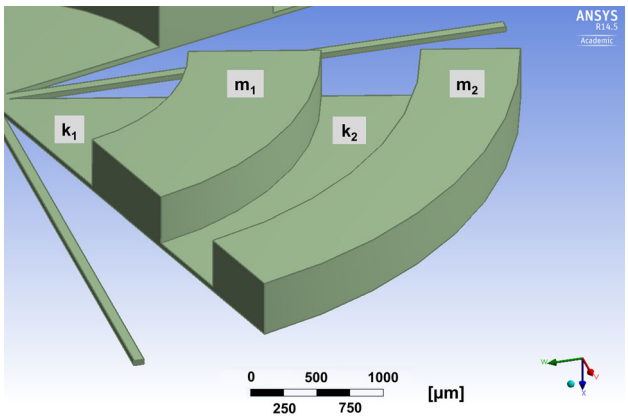

Fig. 4 Workbench bottom view of the double mass–spring system (m_1, k_1; m_2, k_2) implemented by each petal of the FLC EH concept

Such code sections are arranged as follows:

- *Section 1* defined in the geometry of the project flow, states the mechanical properties of AlN (e.g. Young's modulus and Poisson's ratio) as well as the piezoelectric coefficients. The AlN layer is modelled with the SOLID226 (ANSYS Inc. 2012c) accounting for the piezoelectric effect;
- *Section 2* defined in the harmonic response of the project flow, implements the voltage reading at the top and bottom faces of the AlN layer and defines the load resistor [modelled with the CIRCU94 (ANSYS Inc. 2012c) element] connected to the FLC piezoelectric generator;

Fig. 5 GUI of the Ansys Workbench. The project flow, where APDL commands are inserted to model the piezoelectric effect, is highlighted

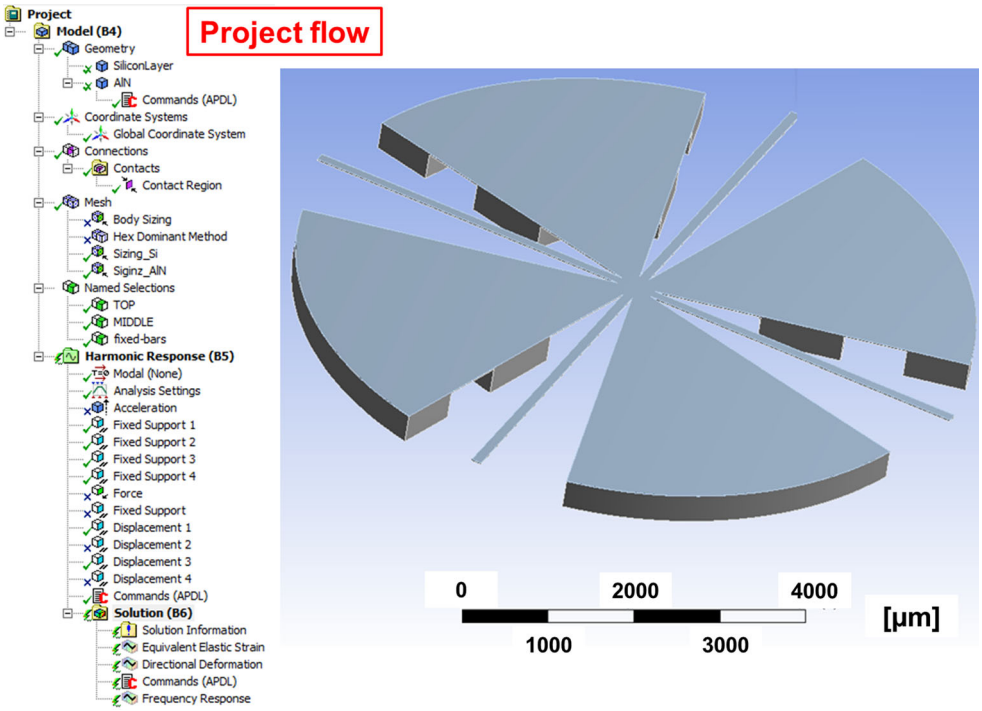

- *Section 3* defined in the solution part of the project flow, finally collects all the commands necessary to save on file the power level generated by the FLC EH at each frequency step defined in the harmonic simulation.

The harmonic simulation of the FLC structure is conducted in the frequency range from 0 to 10 kHz, where typically environmental vibrations are scattered. Concerning mechanical constraints, we anchored the four beams ends (i.e. where the suspended structure is anchored to the surrounding Silicon frame) and imposed a vertical displacement (along Z-axis) of 30 µm to the outer circular edge of two opposite petals, with a phase shift of 120°. This is a reasonable first attempt to reproduce typical conditions to which a physical FLC sample would be subjected to in a real environment, despite other approaches for the stimulation of the mechanical structure are being investigated by the authors (e.g. imposition of acceleration and pressure or random vibration analysis). In the case reported in this paper, the phase shift between the displacement imposed to the two opposite petals is introduced in order to stimulate a deformed shape of the FLC as much asymmetric as possible. Figure 6 shows the vertical deformation (along the Z-axis) of a point on the FLC surface chosen in correspondence with the edge between k_1 and m_1 (see Fig. 4), as predicted by Ansys Workbench up to 500 Hz.

At resonance (i.e. 230 Hz) the vertical displacement of the selected point is 644 µm, showing an amplification of the imposed stimulus (30 µm at the external edges of two opposite petals) of more than 20 times. On the other hand, Figs. 7 and 8 show the distribution of equivalent von-Mises stress and shear stress (on the XY-plane), respectively, through the overall FLC mechanical structure, as predicted by Ansys Workbench at resonance (230 Hz).

The maximum values ranges, i.e. 360 and 155 MPa for the equivalent von-Mises and shear stress, respectively, are well below the critical thresholds investigated in literature for silicon (Saif and MacDonald 1996), indicating that the FLC mechanical structure should reliably operate in the chosen field of application (i.e. environmental vibrations). Looking again at Figs. 7 and 8 it is visible that, as expected, most part of the stress is concentrated in the thin Silicon membranes of petals (springs k_1 and k_2 in Fig. 4).

Figure 9 reports the power generated by the FLC EH when mechanically stimulated as previously discussed. As visible, at resonance the extracted power reaches a peak value of 10.6 µW, which then drops down to a few nW up to 500 Hz.

In order to collect more information on the energy conversion capabilities of the FLC device, we conducted harmonic analysis on a wider range of frequencies. Figure 10 depicts the converted power simulated in Ansys Workbench considering the same conditions of the previous discussed analysis, this time in a frequency range up to 10 kHz.

Apart from the resonant frequency at 230 Hz, already discussed before, the plot now exhibits two additional resonances at 1.96 and 5.65 kHz, corresponding to peaks of generated power of 20 µW and nearly 4 mW, respectively. The latter mode should not be considered as exploitable, since it leads to vertical deformations of the FLC structure larger than 1 mm, which might jeopardise its mechanical robustness. More interestingly, the behaviour at and off resonance should be observed as a whole. If we arbitrarily set a power threshold of 1 µW, as indicated in Fig. 10, assuming it as a watershed imposed by specs, it becomes interesting to analyse what happens around resonant peaks. In light of this consideration, the generated power remains

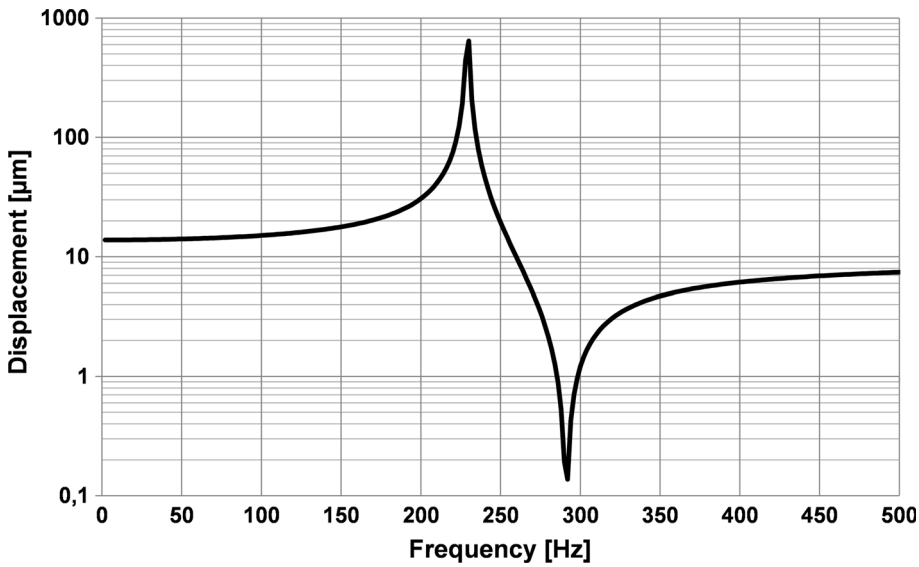

Fig. 6 Vertical deformation (Z-axis) of a point on the FLC surface placed at the edge between k_1 and m_1, predicted by Ansys Workbench

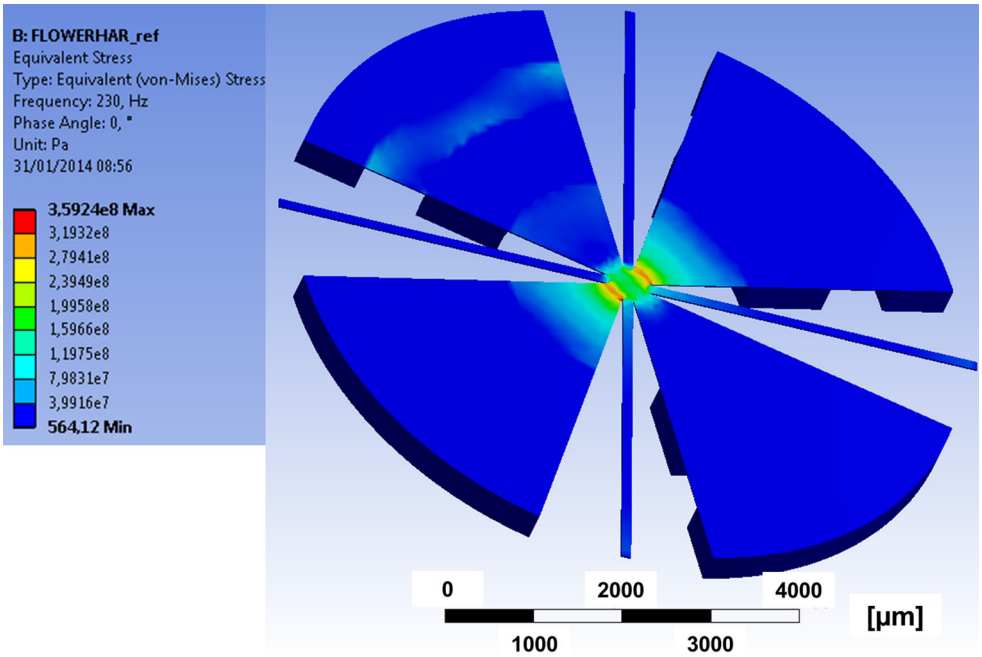

Fig. 7 Distribution of equivalent von-Mises stress through the whole FLC structure at resonance (230 Hz)

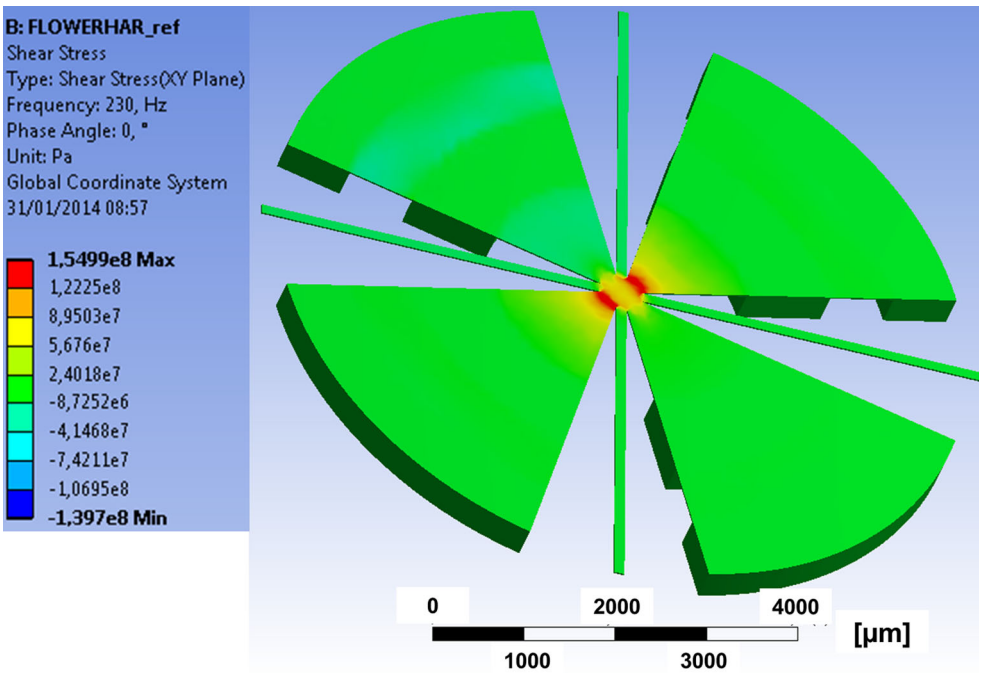

Fig. 8 Distribution of shear stress (on the XY-plane) through the whole FLC structure at resonance (230 Hz)

above 1 µW in a bandwidth of less than 10 Hz around the 230 Hz resonance. Such a bandwidth widens to about 60 Hz around the 1.96 kHz resonant mode, and becomes nearly continuous in the 5–10 kHz range. The just discussed case represents an important indication concerning the way multi-modal resonant response of FLC EH-MEMS concept should be interpreted, i.e. not only focusing on how many resonant frequencies are scattered in the range of vibrations of interest, but paying attention to the extracted power levels between one mode and another, as well. This is, according to our view, the right approach to be adopted in broadening the operability and enhancing the performance when conceiving a novel EH device, and is the address we will follow in the further development of the FLC EH-MEMS design concept.

To conclude this section about multiphysics simulation of the FLC EH-MEMS concept, a few considerations have to be listed. As mentioned before, the analysed FLC configuration has not to be considered as optimal, neither in terms of tailoring the geometry degrees of freedom (DoFs),

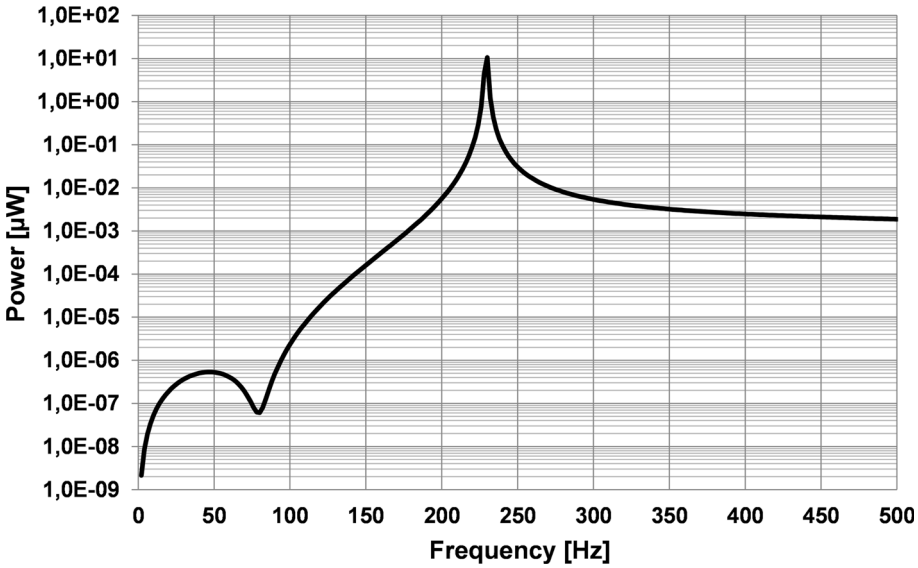

Fig. 9 Plot of the FLC EH output power with the generator loaded by a 100 kΩ resistor. At resonance (230 Hz) the harvested power approaches 11 µW

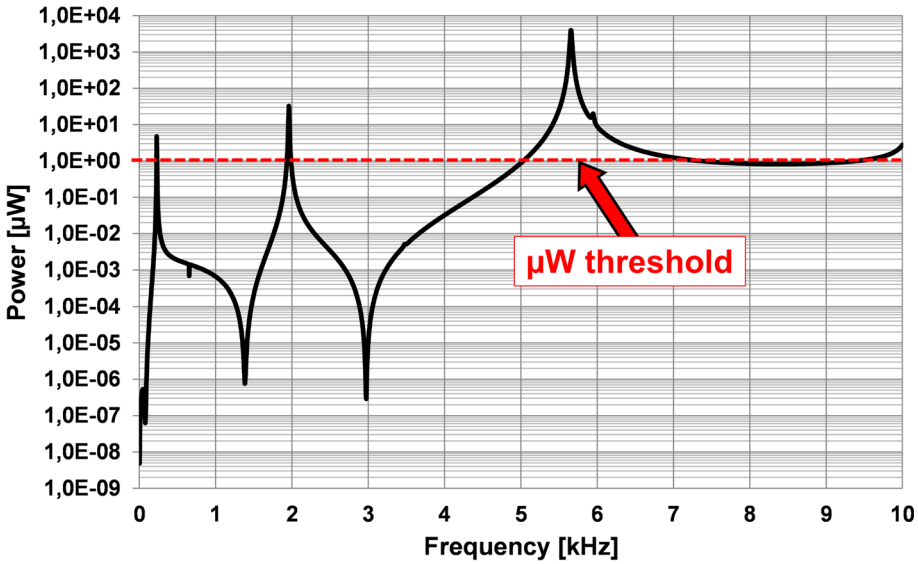

Fig. 10 Plot of the FLC EH output power with the generator loaded by a 100 kΩ resistor up to 10 kHz. The µW threshold is indicated to help reading the graph

nor for what concerns the simulated model. Regarding the first aspect, thorough parametric investigation of all the available DoFs will be conducted prior to the fabrication of physical samples, in order to maximise the harvested power in the frequency range of interest, and to ensure mechanical stability and reliability of the device as well.

On the other hand, some further developments concerning the 3D model and the simulation settings themselves will be operated, aiming to FLC performance enhancement and, on the other side, to a better prediction capability of the Ansys Workbench simulation tool. In the first place, the deployment of AlN layer above the FLC surface will be optimised. In the simulations reported in this paper, the piezoelectric layer was placed on the whole top surface of the device. This represents a worst case scenario, as it is well-known that in case of deformation in opposite direction, like it is in the resonant mode configuration here discussed, charge with different sign can accumulate on the same surface of the AlN material, giving rise to cancellation phenomena that decrease the actual level of power achievable by the structure (Sordo et al. 2015, 2016a, b). To avoid this problem, both in the simulation as well as in the physical device, we are planning to deposit the piezoelectric material separately on petals surface, in such a way that each mass–spring system will work as an independent generator.

5 Conclusions and further works

In this work, we discussed ongoing activities related to the manufacturing of high-performance MEMS-based EHs (energy harvesters) able to convert part of the environmental vibration energy into electrical power by means of piezoelectric effect. The design concept named FLC (four-leaf clover) and already presented by the authors, exploits circular shaped suspended silicon mass–spring systems to enable multiple resonant modes exploitable for energy conversion. FLC EH-MEMS physical samples are fabricated at the ISAS Institute (TU Vienna, Austria). Thereafter, the simulated results presented in this paper were tailored to the characteristics of such a technology. First, experimental activities conducted on sputter deposited aluminium nitride (AlN) piezoelectric thin-film layers were reported, leading to the extraction of the typical material parameters. Afterwards, such measured properties were included in the Ansys Workbench^{TM} finite element method (FEM) tool in order to simulate the multiphysics behaviour of the FLC EH-MEMS with good accuracy. Electromechanical harmonic analysis shows that harvested power levels in the range of several μW are achievable for vibrations up to 10 kHz when the EH is operating in closed-loop conditions (100 kΩ resistive load). These preliminary results are encouraging for the further development of the whole activity.

References

Akiyama M, Kano K, Teshigahara A (2009) Influence of growth temperature and scandium concentration on piezoelectric response of scandium aluminum nitride alloy thin films. Appl Phys Lett 95:1–4. https://doi.org/10.1063/1.3251072

ANSYS Inc. (2012a) DesignModeler user guide. http://www.ansys.com

ANSYS Inc. (2012b) ANSYS parametric design language guide. http://www.ansys.com

ANSYS Inc. (2012c) ANSYS mechanical APDL element reference. http://www.ansys.com

Brennen RA, Pisano AP, Tang WC (1990) Multiple mode micromechanical resonators. In: Proceedings of IEEE MEMS, pp 9–14. https://doi.org/10.1109/memsys.1990.110238

Casset F, Durand C, Dedieu S, Carpentier JF, Gonchond JP, Ancey P, Robert P (2009) 3D multi-frequency MEMS electromechanical resonator design. In: Proceedings of 10th international conference on thermal, mechanical and multi-physics simulation and experiments in microelectronics and microsystems (EuroSimE), pp 1–5. https://doi.org/10.1109/esime.2009.4938416

Chamanian S, Bahrami M, Zangabad RP, Khodaei M, Zarbakhsh P (2012) Wideband capacitive energy harvester based on mechanical frequency-up conversion. In: Proceedings of IEEE sensors applications symposium (SAS), pp 1–4. https://doi.org/10.1109/sas.2012.6166319

Chandrahalim H, Bhave SA (2008) Digitally-tunable mems filter using mechanically-coupled resonator array. In: Proceedings of IEEE MEMS, pp 1020–1023. https://doi.org/10.1109/memsys.2008.4443832

Chidambaram N, Mazzalai A, Muralt P (2012) Comparison of lead zirconate titanate (PZT) thin films for MEMS energy harvester with interdigitated and parallel plate electrodes. In: Proceedings of ISAF/ECAPD/PFM, pp 1–4. https://doi.org/10.1109/isaf.2012.6297833

Coetzee L, Eksteen J (2011) The internet of things—promise for the future? An introduction. In: Proceedings of IST-Africa conference, pp 1–9

Cugat O, Delamare J, Reyne G (2003) Magnetic micro-actuators and systems (MAGMAS). IEEE Trans Magn 39:3607–3612. https://doi.org/10.1109/tmag.2003.816763

Erturk A, Inman DJ (2011) Piezoelectric energy harvesting. Wiley, New York

Fu JL, Nakano Y, Sorenson LD, Ayazi F (2012) Multi-axis AlN-on-Silicon vibration energy harvester with integrated frequency-upconverting transducers. In: Proceedings of IEEE MEMS, pp 1269–1272. https://doi.org/10.1109/memsys.2012.6170388

Galchev T, Aktakka EE, Najafi K (2012) A piezoelectric parametric frequency increased generator for harvesting low-frequency vibrations. IEEE JMEMS 21:1311–1320. https://doi.org/10.1109/jmems.2012.2205901

Goldschmidtboeing F, Wischke M, Eichhorn C, Woias P (2009) Nonlinear effects in piezoelectric vibration harvesters with high coupling factors. In: Proceedings of PowerMEMS, pp 364–367. https://doi.org/10.1177/1045389x09343218

Hackmann G, Guo W, Yan G, Sun Z, Lu C, Dyke S (2014) Cyber-physical codesign of distributed structural health monitoring with wireless sensor networks. IEEE Trans Parallel Distrib Syst 25:63–72. https://doi.org/10.1109/tpds.2013.30

Hagiwara K, Goto M, Iguchi Y, Tajima T, Yasuno Y, Kodama H, Kidokoro K, Suzuki Y (2012) Electret charging method based on soft X-ray photoionization for MEMS transducers. IEEE Trans Dielectr Electr Insul 19:1291–1298. https://doi.org/10.1109/tdei.2012.6260003

Hajati A, Bathurst SP, Lee HJ, Kim SG (2011) Design and fabrication of a nonlinear resonator for ultra wide-bandwidth energy harvesting applications. In: Proceedings of IEEE MEMS, pp 1301–1304. https://doi.org/10.1109/memsys.2011.5734672

Halvorsen E (2013) Fundamental issues in nonlinear wide-band vibration energy harvesting. Phys Rev E 87:1–7. https://doi.org/10.1103/physreve.87.042129

Iannacci J (2017) Microsystem based energy harvesting (EH-MEMS): powering pervasivity of the internet of things (IoT)—a review with focus on mechanical vibrations. Elsevier J King Saud Univ Sci XX:1–9. https://doi.org/10.1016/j.jksus.2017.05.019

Iannacci J, Sordo G (2015) From MEMS to macro-world: a micro-milling machined wideband vibration piezoelectric energy harvester. In: Proceedings of SPIE smart sensors, actuators, and MEMS VII and cyber physical systems, vol 951705, pp 1–10. https://doi.org/10.1117/12.2180143

Iannacci J, Gottardi M, Serra E, Di Criscienzo R, Borrielli A, Bonaldi M (2013) Multi-modal vibration based MEMS energy harvesters for ultra-low power wireless functional nodes. In: Proceedings of SPIE smart sensors, actuators, and MEMS VI, 87630X, vol 8763, pp 1–12. https://doi.org/10.1117/12.2016766

Iannacci J, Sordo G, Gottardi M, Kuenzig T, Schrag G, Wachutka G (2013) An energy harvester concept for electrostatic conversion manufactured in mems surface micromachining technology. In: Proceedings of IEEE international semiconductor conference Dresden-Grenoble, pp 1–4. https://doi.org/10.1109/iscdg.2013.6656310

Iannacci J, Serra E, Di Criscienzo R, Sordo G, Gottardi M, Borrielli A, Bonaldi M, Kuenzig T, Schrag G, Pandraud G, Sarro PM (2014) Multi-modal vibration based MEMS energy harvesters

for ultra-low power wireless functional nodes. Springer Microsyst Technol 20:627–640. https://doi.org/10.1007/s00542-013-1998-2

Iannacci J, Sordo G, Serra E, Schmid U (2016) The MEMS four-leaf clover wideband vibration energy harvesting device: design concept and experimental verification. Springer Microsyst Technol 22:1865–1881. https://doi.org/10.1007/s00542-016-2886-3

Kamierski TJ, Beeby S (2010) Energy harvesting systems: principles, modeling and applications. Springer, Berlin

Karangia R, Jadeja M, Upadhyay C, Chandwani H (2013) Battery-supercapacitor hybrid energy storage system used in electric vehicle. In: Proceedings of international conference on energy efficient technologies for sustainability (ICEETS), pp 688–691. https://doi.org/10.1109/iceets.2013.6533468

Kymissis J, Kendall C, Paradiso J, Gershenfeld N (1998) Parasitic power harvesting in shoes. In: Proceedings of the 2nd international symposium on wearable computers (ISWC), pp 132–139. https://doi.org/10.1109/iswc.1998.729539

Liu SW, Lye SW, Miao JM (2012) Sandwich structured electrostatic/electrets parallel-plate power generator for low acceleration and low frequency vibration energy harvesting. In: Proceedings of IEEE MEMS, pp 1277–1280. https://doi.org/10.1109/memsys.2012.6170390

Miki S, Fujita T, Kotoge T, Jiang YG, Uehara M, Kanda K, Higuchi K, Maenaka K (2012) Electromagnetic energy harvester by using buried NdFeB. In: Proceedings of IEEE MEMS, pp 1221–1224. https://doi.org/10.1109/memsys.2012.6170409

Prescher S, Bourke AK, Koehler F, Martins A, Sereno Ferreira H, Boldt Sousa T, Castro RN, Santos A, Torrent M, Gomis S, Hospedales M, Nelson J (2012) Ubiquitous ambient assisted living solution to promote safer independent living in older adults suffering from co-morbidity. In: Proceedings of the annual international conference of the IEEE engineering in medicine and biology society (EMBC), pp 5118–5121. https://doi.org/10.1109/embc.2012.6347145

Priya S, Inman DJ (eds) (2009) Energy harvesting technologies. Springer Science, Berlin

Roundy S, Wright PK, Rabaey JM (2004) Energy scavenging for wireless sensor networks: with special focus on vibrations. Kluwer Academic Publishers, Dordrecht

Sah RE, Kirste L, Baeumler M, Hiesinger P, Cimalla V, Lebedev V, Baumann H, Zschau H-E (2010) Residual stress stability in fiber textured stoichiometric AlN film grown using rf magnetron sputtering. J Vacuum Sci Technol A Vac Surf Films 28:394–399. https://doi.org/10.1116/1.3360299

Saif MTA, MacDonald NC (1996) Micro mechanical single crystal silicon fracture studies torsion and bending. In: Proceedings of IEEE MEMS, pp 105–109. https://doi.org/10.1109/memsys.1996.493837

Schalko J, Beigelbeck R, Stifter M, Schneider M, Bittner A, Schmid U (2011) Improved load-deflection method for the extraction of elastomechanical properties of circularly shaped thin-film diaphragms. In: Proceedings of SPIE, vol 8066, pp 1–8. https://doi.org/10.1117/12.886824

Solazzi F, Iannacci J, Faes A, Giacomozzi F, Margesin B, Tazzoli A, Meneghesso G (2011) Modeling and characterization of a circular-shaped energy scavenger in MEMS surface micromachining technology. In: Proceedings of SPIE microtechnologies conference, vol 8066, pp 1–8. https://doi.org/10.1117/12.887559

Sordo G, Serra E, Schmid U, Iannacci J (2015) Optimization method for designing multimodal piezoelectric MEMS energy harvesters. In: Proceedings of SPIE smart sensors, actuators, and MEMS VII and cyber physical systems, vol 95170O, pp 1–8. https://doi.org/10.1117/12.2180953

Sordo G, Iannacci J, Schmid U (2016a) Study on the effectiveness of different electrode geometries for sputtered aluminium nitride-based MEMS energy harvesters. In: Proceedings of symposium on design, test, integration and packaging of MEMS and MOEMS (DTIP), pp 213–216. https://doi.org/10.1109/dtip.2016.7514871

Sordo G, Serra E, Schmid U, Iannacci J (2016b) Optimization method for designing multimodal piezoelectric MEMS energy harvesters. Springer Microsyst Technol 22:1811–1820. https://doi.org/10.1007/s00542-016-2848-9

Suzuki M, Matsushita N, Hirata T, Yoneya R, Onishi J, Wada T, Takahashi T, Nishida T, Yoshikawa Y, Aoyagi S (2011) Fabrication of highly dielectric nano-$BaTiO_3$/epoxy-resin composite plate having trenches by mold casting and its application to capacitive energy harvesting. In: Proceedings of 16th IEEE international solid-state sensors, actuators and microsystems conference (TRANSDUCERS), pp 2642–2645. https://doi.org/10.1109/transducers.2011.5969873

Tao K, Ding G, Wang P, Yang Z, Wang Y (2012) Fully integrated micro electromagnetic vibration energy harvesters with micro-patterning of bonded magnets. In: Proceedings of IEEE MEMS, pp 1237–1240. https://doi.org/10.1109/memsys.2012.6170413

Todorov G, Valtchev S, Todorov T, Ivanov I, Klaassens B (2011) Tuning techniques for kinetic MEMS energy harvesters. In: Proceedings of IEEE 33rd international telecommunications energy conference (INTELEC), pp 1–6, 2011. https://doi.org/10.1109/intlec.2011.6099874

Wagner J-M, Bechstedt F (2002) Properties of strained wurtzite GaN and AlN: ab initio studies. Phys Rev B 66:1–20. https://doi.org/10.1103/physrevb.66.115202

Wan ZG, Tan YK, Yuen C (2011) Review on energy harvesting and energy management for sustainable wireless sensor networks. In: Proceedings of the IEEE 13th international conference on communication technology (ICCT), pp 362–367. https://doi.org/10.1109/icct.2011.6157897

Zhu D (2011) Vibration energy harvesting: machinery vibration, human movement and flow induced vibration. In: Tan YK (ed) Sustainable energy harvesting technologies—past, present and future. InTech, Rijeka

Zorlu O, Topal ET, Külah H (2011) A vibration-based electromagnetic energy harvester using mechanical frequency up-conversion method. IEEE Sens J 11:481–488. https://doi.org/10.1109/jsen.2010.2059007

Zukauskaite A, Wingqvist G, Palisaitis J, Jensen J, Persson Per OÅ, Matloub R, Muralt P, Kim Y, Birch J, Hultman L (2012) Microstructure and dielectric properties of piezoelectric magnetron sputtered w-$Sc_xAl_{1-x}N$ thin films. J Appl Phys 111:1–7. https://doi.org/10.1063/1.4714220